Journal of Structural Geology 31 (2009) 1443–1457

Contents lists available at ScienceDirect

Journal of Structural Geology

journal homepage: www.elsevier.com/locate/jsg

# Kinematic models of basement/cover interaction: Insights from the Malargüe fold and thrust belt, Mendoza, Argentina

Laura Giambiagi [a,*], Matías Ghiglione [b], Ernesto Cristallini [c], Germán Bottesi [d]

[a] CONICET-IANIGLA Centro Regional de Investigaciones Científicas y Tecnológicas, Parque San Martín s/n, 5500 Mendoza, Argentina
[b] Laboratorio de Tectónica Andina, Universidad de Buenos Aires. Ciudad Universitaria, Pabellón II, C1426EHA, Argentina
[c] Laboratorio de Modelado Geológico (LaMoGe), Universidad de Buenos Aires, Ciudad Universitaria, Pabellón II, C1426EHA, Argentina
[d] YPF S.A., Esmeralda 255, Buenos Aires, C1035ABE, Argentina

ARTICLE INFO

*Article history:*
Received 25 September 2008
Received in revised form
28 August 2009
Accepted 7 October 2009
Available online 14 October 2009

*Keywords:*
Thin-skinned
Thick-skinned fold and thrust belt
Propagation/slip ratio
Andes

ABSTRACT

We investigate through natural examples from the Malargüe fold and thrust belt the manner in which the basement structures interact with the cover in a thick-skinned fold and thrust belt. Our work suggests that there is a broad spectrum of basement–cover interaction mechanisms with two end-members: coupled and uncoupled interactions. The kind of bonding between basement and cover is related to the propagation to slip ratio ($p/s$), because high values of this ratio indicate rapid forward propagation of shortening into the cover, while low values favour welding between basement and cover structures. We analyse the factors controlling the kinematics of basement–cover deformation, and find that not only the strength of the cover, its thickness, and its mechanical anisotropy control the $p/s$ and basement–cover bonding, but also the strain rate, the thickness of synorogenic strata, and the presence of pre-existing faults.



## 1. Introduction

Thin- and thick-skinned fold and thrust belts show an intimate relationship between faulting and folding. This relationship has led to numerous quantitative fault-related folding models based primarily on structural geometry from which kinematics is often inferred: fault-bend folding, fault-propagation folding, detachment folding and trishear fault-propagation folding (Suppe, 1983; Williams and Chapman, 1983; Suppe and Medwedeff, 1984; Jamison, 1987; Chester and Chester, 1990; Mitra, 1990; Wichkam, 1995; Erslev, 1991; Hardy and Ford, 1997; Allmendinger, 1998). Because of their geometrical basis, however, the models do not predict why or when a particular process will occur (Chester et al., 1991). They are basically differentiated on the basis of the relative timing of fault and fold initiation. While in fault-bend folding a fault with a ramp-flat trajectory must be previous to slip, in the fault-propagation fold and trishear models slip and faulting are synchronous, with folds growing as faults progressively cut up-section (Suppe and Medwedeff, 1990; Mitra, 1990; Erslev, 1991). In practice, distinction between the various kinematic models may be difficult because these models are strictly kinematic ones, lacking a complete mechanical foundation (Allmendinger et al., 2004), although in recent years, a variety of different mechanical models have been applied in an effort to better understand the physical meaning of kinematic models (Hardy and Ford, 1997; Johnson and Johnson, 2002; Cardozo et al., 2003, 2005; Finch et al., 2003; Hardy and Finch, 2007).

This paper investigates different basement–cover interaction mechanisms affecting a thick-skinned fold and thrust belt in the Southern Central Andes, the Malargüe fold and thrust belt (Malargüe FTB). This belt constitutes an outstanding natural laboratory due to a combination of excellent outcrops and profuse subsurface information. The coexistence of both thin- and thick-skinned structures along the same belt, as well as thick wedges of synorogenic strata, makes the belt suitable for studying the three-dimensional geometry and evolution of thick- and thin-skinned structural interactions. The aim of this paper is to characterize in detail the three-dimensional structure of the Malargüe FTB in order to determine the kinematics of basement-cored structures and the mechanisms of basement–cover interaction, and to address the factors controlling these mechanisms. To achieve this, we investigate displacement transfers and kinematic links between basement faults and sedimentary cover thrusts, which will provide new insights into fault-related folding kinematics in thick-skinned fold and thrust belts.

* Corresponding author. Fax: +54 261 5244220.
*E-mail addresses:* lgiambia@lab.cricyt.edu.ar (L. Giambiagi), matias@gl.fcen.uba.ar (M. Ghiglione), ecristallini@gmail.com (E. Cristallini), glbottesio@repsolypf.com (G. Bottesi).

0191-8141/$ – see front matter © 2009 Elsevier Ltd. All rights reserved.
doi:10.1016/j.jsg.2009.10.006

## 2. Fault–fold interaction

### 2.1. Kinematic modelling algorithms

Modelling algorithms for fault restorations are techniques used in quantitative structural analysis to study the effects of fault geometry on hanging wall and footwall deformation. They provide an effective tool for validating structural interpretations constructed from geological and geophysical data. Despite the fact that they involve simple mechanisms to simulate deformation, they are easy to implement and they conserve the area of the section in a restored state. These algorithms are based on deformational mechanisms, such as flexural slip (bedding-parallel slip – Fig. 1a), flexural flow (fault-parallel shear or fault-parallel flow – Fig. 1b), antithetic and synthetic shear oblique to bedding (Fig. 1c), and trishear (triangular shear) (Fig. 1d).

The flexural slip algorithm allows the layers to slide relative to each other, maintaining line length and bed thickness constant (Fig. 1a) (Kane et al., 1997). The fault-bend fold model (Suppe, 1983) assumes flexural slip as the main deformation mechanism, and results in passive folding above a pre-existing fault.

The flexural flow or fault-parallel flow is an algorithm best suited for modelling hanging wall movement on faults where the majority of the deformation occurs discretely between bed interfaces (Fig. 1b, Sanderson, 1982; Egan et al., 1999). It models structures where deformation is accommodated by fault-parallel shear in the hanging wall, assuming particle flow parallel to the fault surface. The mechanism is similar to flexural slip folding, except that in flexural flow, beds do not conserve their thickness unless an angular shear is applied. The algorithm can be applied to thin-skinned fold and thrust belts, extensional regions and mixed-mode settings, and it is best to model fault-bend folds (Egan et al., 1999).

The inclined shear algorithm geometrically models the relationship between fault geometry and hanging wall deformation using vertical or inclined shear vectors, which enable the hanging wall to deform via a defined shear angle (White et al., 1986; Dula, 1991; Withjack and Peterson, 1993). The algorithm models diffuse deformation throughout the hanging wall rather than discrete slip between beds (Fig. 1c). It can be applied to extensional tectonics where anticlinal rollover structures have developed on non-planar listric normal faults, inversion and growth faults where the thickness of beds may vary (Buddin et al., 1997; Bulnes and McClay, 1998). It can also be effective for restoring basement listric faults where the curvature of the fault is responsible for deformation that occurs in the hanging wall.

Both fault-bend and fault-propagation folding models infer that flexural slip parallel folding is the main mechanism of deformation (Suppe and Medwedeff, 1990). In recent years, however, the trishear kinematic model of fault-propagation folding has been applied as an alternative to the flexural slip fault-propagation fold models and it appears to explain well the geometric development and finite strain of some folds (Erslev, 1991; Hardy and Ford, 1997; Allmendinger, 1998; Zehnder and Allmendinger, 2000; Hardy and Allmendinger, in press). This method is derived from velocity descriptions of deformation. According to trishear, the slip along a propagating fault is accommodated by distributed strain within a triangular zone of deformation that radiates from the fault tip (Fig. 1d). In contrast to the kink-band models, the trishear deformation is driven by five independent parameters: fault slip, propagation to slip ratio ($p/s$), trishear angle, the amount of slip per deformation step, and the orientation of the trishear zone to the fault; although the $p/s$ and trishear angle appear to be inversely correlated (Allmendinger et al., 2004).

### 2.2. Propagation to slip ratio (p/s)

Because the processes of fault propagation and displacement cannot generally be observed directly in natural structures, several theoretical analyses have been used to estimate the relative importance of these processes. One of these analyses was proposed by Williams and Chapman (1983) who introduced the slip to propagation ratio ($s/p$ ratio), where $s$ is the fault slip (displacement) and $p$ is the propagated fault length. Rather than comparing fold shape and fault geometry, these authors proposed an alternative procedure for the analysis of fault–fold relations, considering the displacement gradient along a fault surface and the relationship of fault displacement and fault length. They indicated an end-member behavior between propagating folds with no displacement ($s/p = 0$) and displacing faults with no propagation ($s/p = \infty$). Later on, a similar parameter, the $p/s$ ratio, was introduced in the trishear kinematic model (Hardy and Ford, 1997; Allmendinger, 1998;

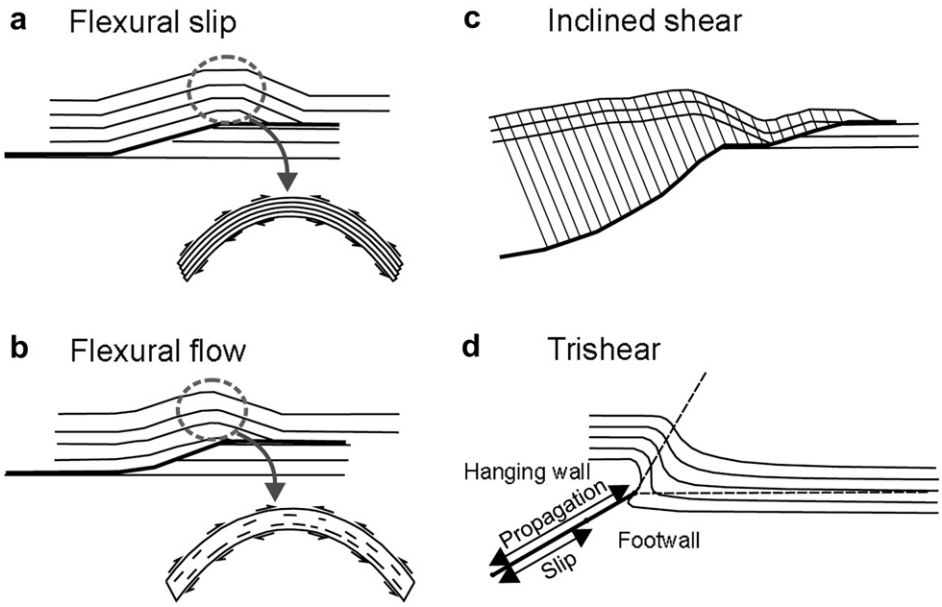


**Fig. 1.** Kinematic algorithms for fault restoration.

Allmendinger and Shaw, 2000; Fig. 1D). In this model, low values of *p*/*s* result in pronounced forelimb thickening and tight folding in the trishear zone, whereas high values of *p*/*s* result in open folding (Hardy and Ford, 1997; Allmendinger, 1998).

Although rarely acknowledged, all kinematic modes of fault-related folding imply a specific relationship between the relative rates of fault propagation and fault slip. As Hardy and Ford (1997) pointed out, the style of folding primarily depends on the *p*/*s* ratio. Inherent in Suppe's fault-bend folding is the assumption that the fault exists at the earliest stages of displacement, with an infinite *p*/*s* ratio. In flexural slip, constant thickness fault propagation folds *p*/*s* is related to fault step-up angle (Hardy, 1997). For higher values of this angle, a fault will propagate faster for a given amount of slip. The development of folds above fault tips is favoured when the rate of fault growth is low relative to the slip rate (Suppe and Medwedeff, 1984), or when the fault tip is pinned as fault slip increases (Wichkam, 1995). Moreover, a combination of low *p*/*s* ratio follows by high *p*/*s* ratio, or vice versa, could account for very diverse fold-thrust relationships observed in natural examples.

The physical properties that control the *p*/*s* ratio are not well known, but factors such as lithology, mechanical stratigraphy, cover and growth strata thicknesses, strain rate, and fluid pressure are thought to be important (Muraoka and Kamata, 1983; Erslev and Rogers, 1993; Hedlund, 1997; Mitra and Mount, 1998; Allmendinger, 1998; Erickson et al., 2001; Cardozo et al., 2003; Finch et al., 2003; Strayer et al., 2004; Hardy and Finch, 2006). We document in the next sections very different *p*/*s* ratio values during the development of the Malargüe FTB structures both along and across strike, and discuss the physical properties that might have controlled them.

## 3. Geological background

The Malargüe FTB is one of several Cenozoic contractional belts located in the Andean foothills in central-western Argentina. It extends south from the Maipo volcano area at 34°S to the Grande river at 36°S (Fig. 2). The Malargüe FTB has been classically identified as a hybrid fold and thrust belt with basement thrust sheets transferring shortening to the thick Meso-Cenozoic sedimentary cover (Kozlowski et al., 1993; Manceda and Figueroa, 1995; Silvestro and Atencio, in press; Giambiagi et al., 2008).

On the basis of mechanical stratigraphy, the lithostratigrafic units of the belt can be divided into five structural packages; from bottom to top these are (Fig. 3): (1) Proterozoic to Lower Triassic metamorphic, plutonic and volcanic rocks which constitute the crystalline basement of the thrust belt; (2) Upper Triassic to Lower Jurassic continental rift sequences; (3) Middle Jurassic to Lower Cretaceous platform sequences from the sag stage; (4) Upper Cretaceous to Paleogene continental and marine strata; and (5) Neogene-Quaternary synorogenic continental strata and volcanic rocks.

In the Malargüe and Valenciana Triassic–Jurassic extensional depocentres, synrift deposits consist of more than 800 m of fluvio-lacustrine and marine sequences distributed accordingly to the rift-related major normal faults. In the Palauco area, synrift deposits consist of more than 1000 m of continental sedimentary rocks, volcaniclastic and volcanic deposits.

During the Middle Jurassic to Early Cretaceous, the Neuquén back-arc basin was filled by clastic, carbonate, and evaporite systems deposited during the sag stage. These deposits are more than 4000 m thick in the western part of the study area, and taper toward the east, where they are less than 1000 m thick. The Upper Cretaceous to Paleogene deposits belong to a foreland basin developed as a result of compression in the Andean Cordillera, and consist of competent continental sandstones and conglomerates, marine limestones, and lacustrine and playa lake clastics.

The Neogene synorogenic strata were deposited in foreland and broken-foreland basin settings and consist of more than 1200 m of andesitic pyroclastic breccias, basaltic and andesitic lavas, conglomerates and sandstones, deposited between 18 and 3 Ma (Silvestro et al., 2005; Silvestro and Atencio, in press). These deposits are preserved all around the Malargüe FTB, especially in the central and eastern part of the belt (Fig. 2).

## 4. Methodology

To characterize the 3D structure of the Malargüe FTB, the following approaches were used: (1) geological mapping of outcropping structures integrated with previously published (Groeber, 1937; Dessanti, 1973; Gulisano and Gutierrez Pleimling, 1994; Dicarlo and Cristallini, 2007; Yagupsky et al., 2007, 2008) and unpublished (Legarreta et al., 1985; Kozlowski et al., 1989) geological maps, (2) integration of previous studies on the Triassic–Jurassic rift architecture (Giambiagi et al., in press), (3) interpretation of 563 seismic reflection lines and 163 wells (Fig. 4), (4) construction of structural cross-sections parallel to the tectonic transport direction, and (5) kinematic modelling of basement–cover interaction for the main basement structures.

A series of 15 detailed cross-sections were constructed through the fold and thrust belt using regional data, section-balancing techniques, and the geological interpretation of seismic and well data (Figs. 2, 5 and 6). We produced forward models using different two-dimensional area-balancing techniques for each major structure and searched the best geometric match between model and observation. We analysed the folding mechanisms for each fault–fold basement-involved system, determining the best-fitting kinematic model and distinguishing between flexural slip, flexural flow, inclined shear and trishear mechanisms. Fault parameters, including fault dip, depth, length, and amount of slip, were systematically varied to fix the observed structure. Forward modelling permits to change various parameters at any time during a model run. We constructed our models with the 2D-modelling software *MOVE 2009.1* (© Midland Valley Exploration Ltd.). It has been estimated that the thrusts merge into a 9–10 km depth detachment located within the basement. This depth to detachment was calculated by carrying the surface and subsurface geology to depth maintaining the dips of the stratigraphic packages, and considering the regional position of basal detachment (Manceda and Figueroa, 1995; Allmendinger et al., 2004; Zapata and Folguera, 2005; Giambiagi et al., 2008; Silvestro and Atencio, in press). A 10-km-detachment was independently calculated from seismological data (Farías et al., 2005).

We estimated the amount of shortening in the cover and in the basement for each main structure. To achieve this, we used two points located at a shallow level within the basement (1 km below basement–cover interface) and two points located at the base of the Upper Jurassic black shales. We measured the distance between both pair of points in the cross-sections ($l_f$) and in the reconstruction ($l_0$), and estimated the amount of shortening in the cover and in the basement by comparing these distances ($l_{0-}\ l_f$) and its percentage [$l_{0-}\ l_f$]/$l_0$.

We measured the *p*/*s* ratio taking into account the principal structures affecting the basement. In the western sector of the belt, there is a complex relationship between different basement faults and deformation in the cover. Although the deformed zone is characterized by parallel folding and imbricate faulting, we can model the broader scale geometries with trishear to investigate the *p*/*s* ratio because only trishear treats *p*/*s* as an independent parameter (Hardy and Allmendinger, in press). We only measure the *p*/*s* ratio for the principal fault connecting the deformation in the basement with that of the cover. The hanging walls of these faults are affected by faults which were not measured for this

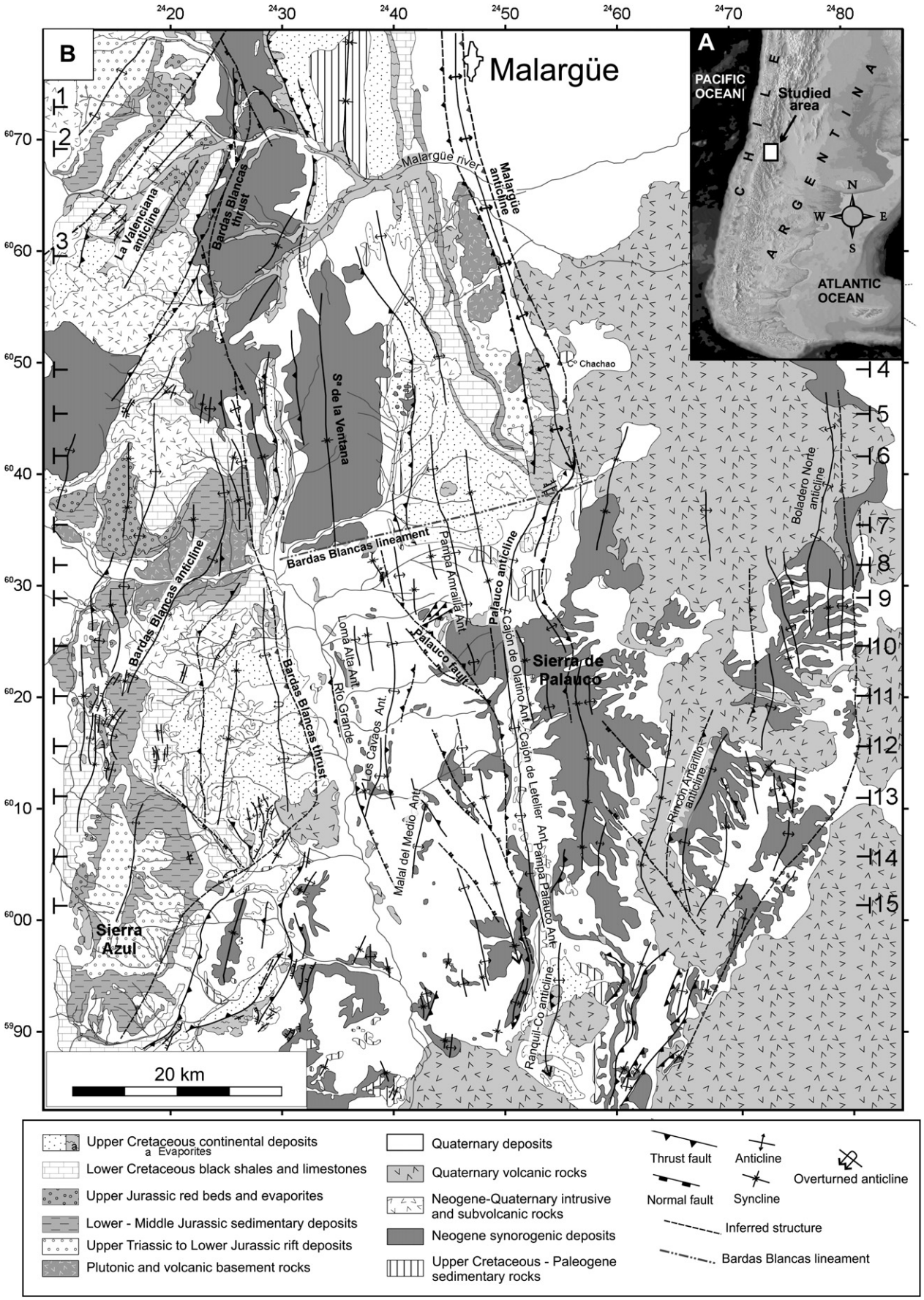


**Fig. 2.** (A) Location map, and (B) geologic map of the Malargüe FTB, showing location of cross-sections 1–15. Modified from Legarreta et al. (1985), Kozlowski et al. (1989), Yagupsky et al. (2007), and Giambiagi et al. (in press).

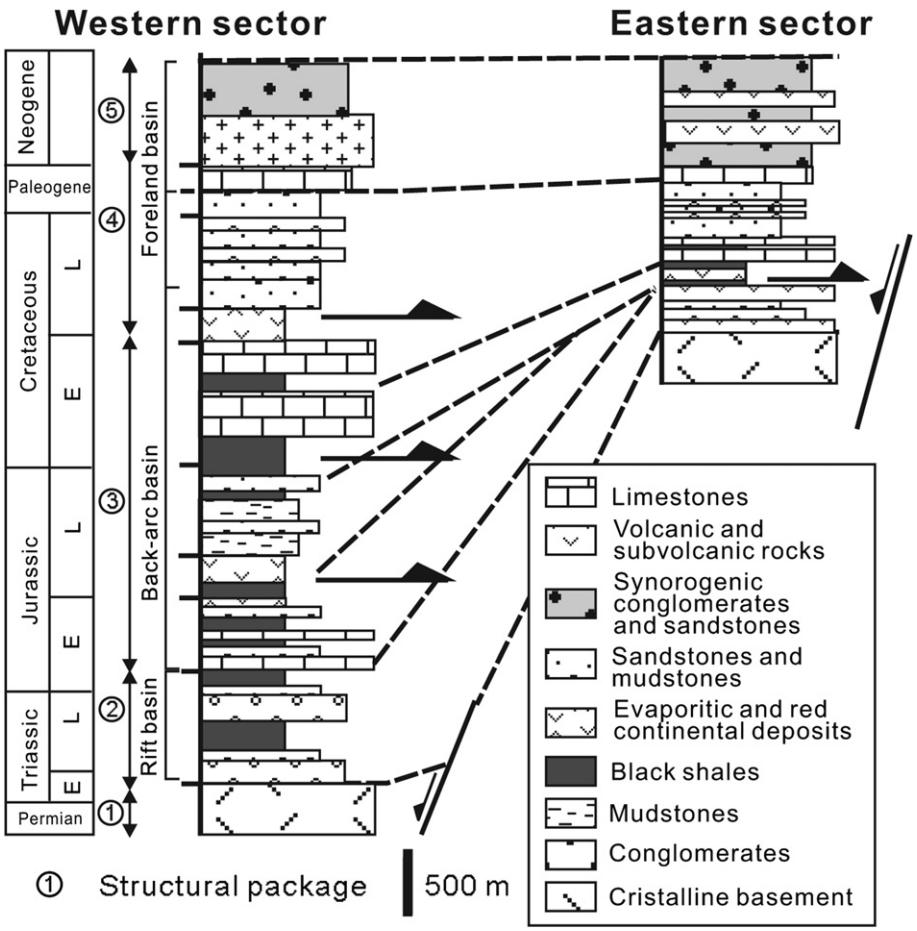


**Fig. 3.** Simplified stratigraphic columns showing the main structural packages and their correlation between western and eastern sectors of the Malargüe FTB.

analysis. Because *p*/*s* and trishear angle are inversely correlated and a small change in *p*/*s* has a more profound change on fold shape than does a small change in trishear angle (Allmendinger et al., 2004), we evaluate the degree of control of both parameters over the final geometry by fixing the trishear angle and evaluating variations in *p*/*s*, and vice versa.

## 5. Structural style

The Malargüe FTB is deformed by three deeply seated structures with involvement of the rigid basement. They are the Malargüe and Palauco anticlines to the east and the Bardas Blancas fault system to the west (Figs. 2, 5 and 6). Detailed observations on the structural cross-sections and the relation between structures and synorogenic strata suggest that the thrust belt was developed during a main episode of faulting between Middle Miocene and Late Pliocene (Giambiagi et al., 2008; Silvestro and Atencio, in press). Numerous extensional features inherited from the Triassic–Jurassic rifting episode contribute to the overall structural grain of the area (Manceda and Figueroa, 1995; Giambiagi et al., 2008, in press; Yagupsky et al., 2008). This is specially the case in the Malargüe and Palauco areas, where pre-existing normal faults are interpreted to have controlled the localization of some faults and the vergence of the compressional deformation.

### 5.1. Malargüe anticline

The Malargüe anticline is an east-vergent, asymmetric fold, plunging shallowly to the south. It exhibits a gently dipping backlimb and a very steeply dipping forelimb, and it exposes Permo-Triassic volcanic basement rocks (Figs. 2 and 5). The main characteristic of the anticline is that its backlimb shows little deformation with no detachment along the basement–cover interface, while the forelimb steepens as it approaches the fault tip, where it is overturned. Petroleum logs identify important bed thickness variations in the forelimb, with a downward progressive fold tightening and truncation of footwall syncline. The subsurface data also indicate that shortening decreases up-section into a triangle zone, and that the basement–cover surface is folded.

Six cross-sections (1–6 in Fig. 5) display two-dimensional geometries that markedly vary along strike from north to south. Cross-sections 1–4 show a strongly asymmetric fold with associated east-vergent faults and a backthrust, while cross-sections 5 and 6 show an open and more symmetrical fold with associated small-displacement faults. The structure has an overall north-south trend, but in the cross-sections 3–5 it shows a NNW trend (Fig. 2). In none of the cross-sections does the fold-related fault propagate into the foreland; instead, it forms a blind fault below the Cretaceous continental strata or the Cenozoic synorogenic deposits (Fig. 7).

We interpreted the folding of the basement surface as reflecting fault propagation from a point three kilometres below that basement–cover interface. The point from which the fault propagated was obtained from trishear modelling (Fig. 7D) and could correspond to the propagation point of a short-cut fault, created by the compression of the upward-steepening normal fault.

The fold is offset by another fault that cuts through the shallow deeping backlimb. This fault is considered to be a breakout fault or

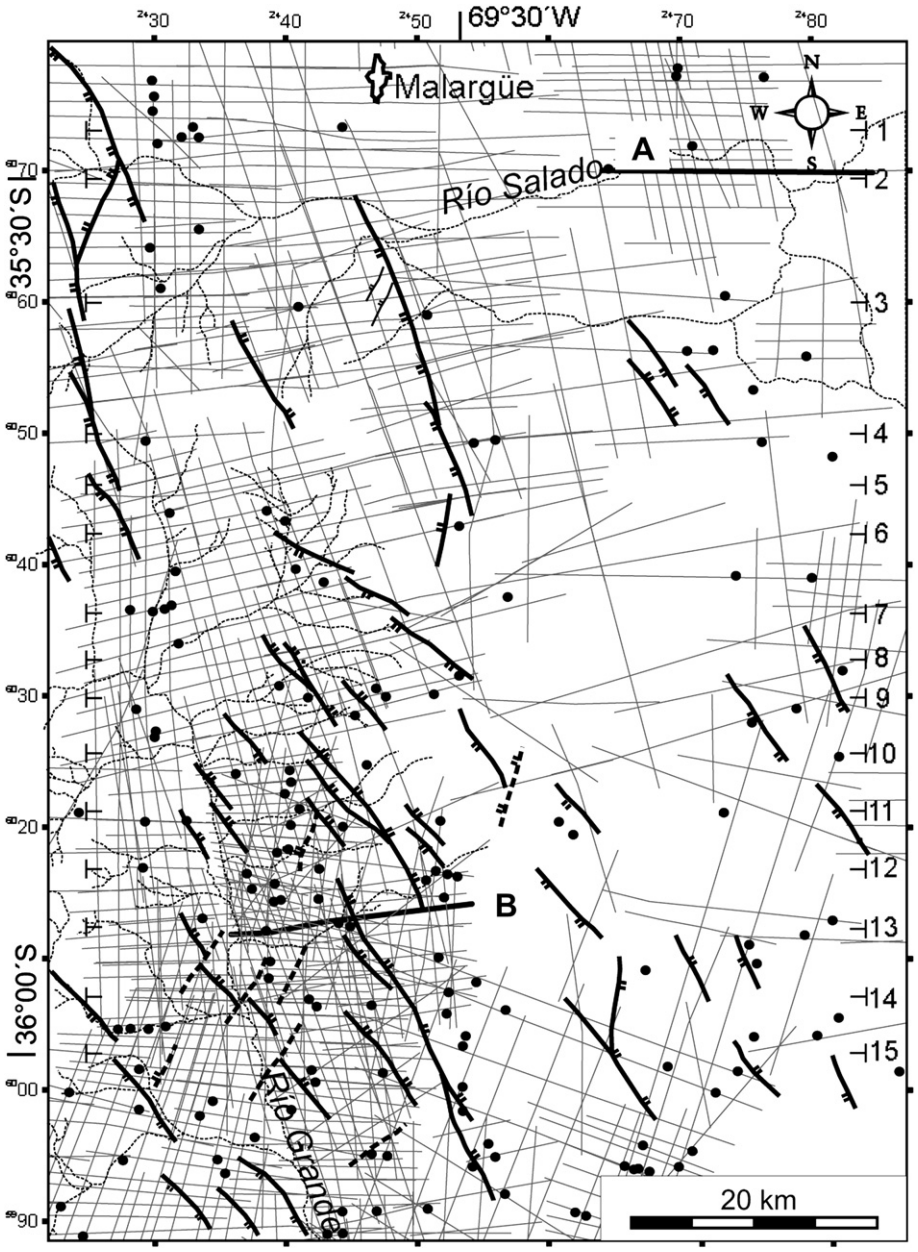


**Fig. 4.** Map with seismic line and well locations, where the pre-existing normal faults were drawn (Giambiagi et al., in press). (A) and (B) Location of seismic lines in Figs. 7 and 8, respectively.

breakthrough fault (Mitra, 1990; Suppe and Medwedeff, 1990), which results when the fault associated with a fault-propagation fold cuts rapidly across the stratigraphic section, abandoning the fold as a relic of the former position of the tip line. The tip line has moved rapidly away from the structure and this could only happen if the propagation is much larger that the slip (Allmendinger, 1998). The difference in *p*/*s* ratio between the Malargüe fault and the breakout fault is interpreted as due to reactivation of a pre-existing structure. Because this breakout fault is associated with Triassic–Jurassic synrift strata outcroping in sections 3–5, this segment of the fault is interpreted to belong to a Mesozoic listric normal fault, reactivated during Cenozoic compression. The NNW structural trend of the Malargüe anticline in sections 3–5 (Fig. 2) could be related to the trend of previous synrift normal faults. This is in agreement with NNW-trending extensional structures of the Neuquén basin (Giambiagi et al., in press).

The Malargüe anticline was previously interpreted as a fault-bend fold (Manceda and Figueroa, 1995; Nocioni, 1996), and as a fault-propagation fold (Silvestro and Atencio, in press). We propose an alternative model with the positive reactivation of a listric normal fault and the development of a short-cut fault in the steep deepening part of the fault (Fig. 7D). The complex fold geometry has been explained by a triangular shear zone radiating from the tip of the short-cut fault. In this model the progressive limb rotation during folding occurs until the structure locks or the stress was high enough to generate faulting in the steeply dipping, reactivated normal fault. In this stage, the pre-existing Malargüe fault reactivates and propagates with a high *p*/*s* (8) from the basal detachment across basement rocks with no associated folding, producing a breakout fault.

Sedimentation was coeval with the contractional deformation, leading to the preservation of growth strata. In the eastern flank of

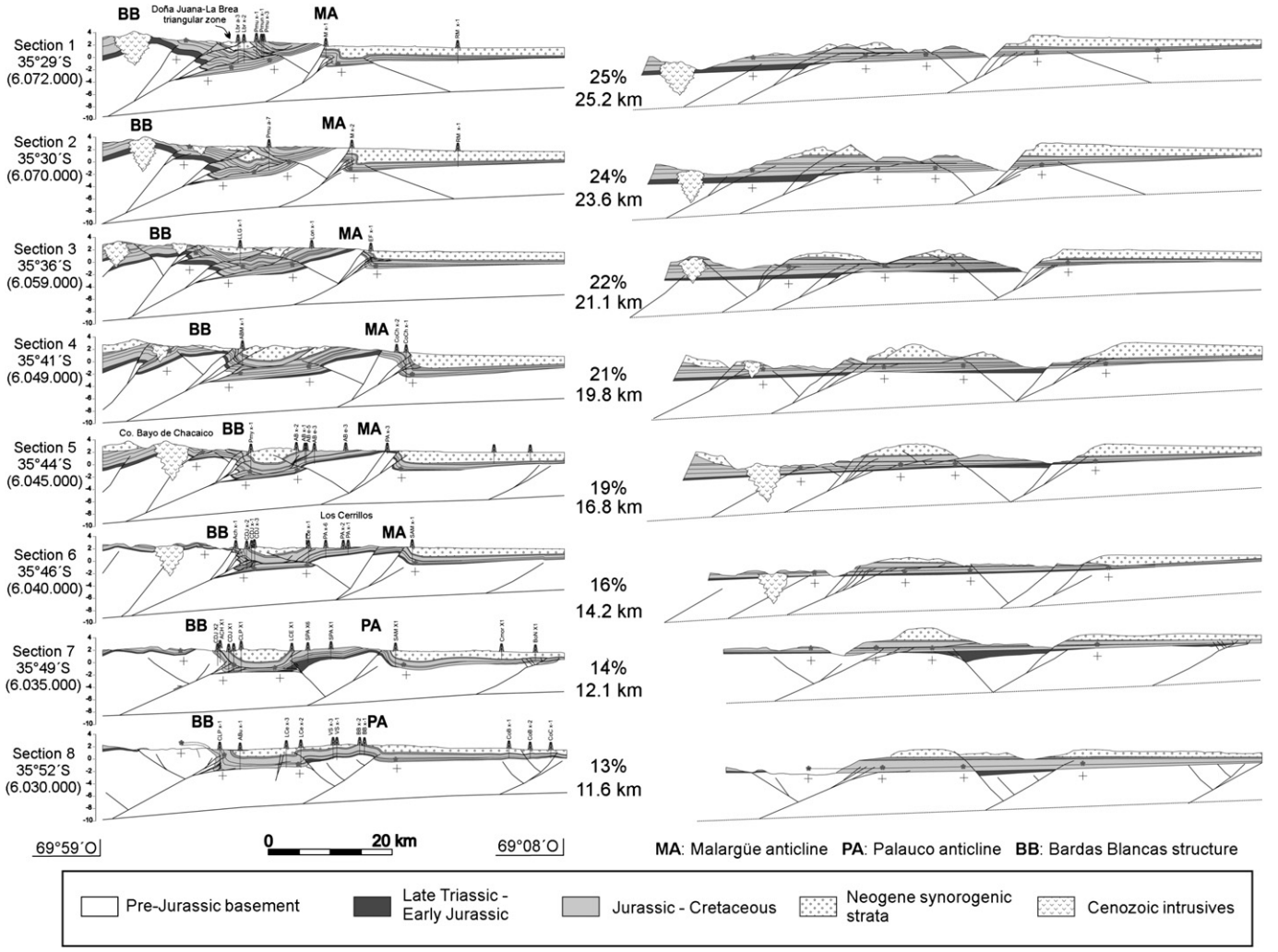


**Fig. 5.** Balanced cross-sections 1–8 of the Malargüe FTB, between 35°29′ and 35°52′S. The amounts of horizontal shortening of the main structures have been obtained measuring distance between black (basement) and grey (cover) crosses in deformed and restored cross-sections.

the fold, growth strata display wedge geometry with basal onlap and divergent reflections (Silvestro et al., 2005, Silvestro and Atencio, in press) (Fig. 7, B and C). The observations on the geometries of growth strata give us another parameter to distinguish between the different fold models. The asymmetric pattern of rotated constant thickness backlimb strata and rotated, onlapping and overlapping forelimb strata is similar to a fault-propagation fold (Hardy and Poblet, 1995; Ford et al., 1997), and indicates progressive forelimb rotation and trishear-like fault-propagation folding (Silvestro and Kraemer, 2005).

### 5.2. Palauco anticline

The Palauco anticline is a complex N–S trending basement structure, characterized by a series of double plunging anticlines, called from north to south: Pampa Amarilla, Cajón de Olatino, Cajón de Letelier, Pampa Palauco and Ranquil-Co (Figs. 2, 5 and 6). These folds are flanked by two opposite-verging faults in its northern culmination (Sections 7–10), whereas to the south (Sections 11–15) the westward verging Palauco backthrust accommodates most of the shortening while the eastward vergent fault loses expression (Fig. 6). The Palauco backthrust propagates up to the surface south of section 10, coinciding with an abrupt increase in shortening that produces up to 2000 m of vertical displacement and an increase in fault dip. In this sector, the synrift deposits drilled by exploratory wells in the core of the anticlines (CDO x1–x2 – Fig. 6) reach up to 1000 m thickness. Although it has been debated for a long time whether or not the Palauco backthrust is the result of the positive inversion of a rift fault, it is suggested from subsurface data (Fig. 8) and surface structural mapping that it is made of en echelon previously normal fault segments oriented obliquely to the Cenozoic compressional direction (Figs. 2 and 4).

To understand the fault–fold relationship and the mechanism of deformation in the Palauco anticline, we modelled the structure with the trishear algorithm with different amount of *p*/*s* ratio north and south of cross-section 11 (Fig. 9). In the northern part, between cross-sections 7 and 10, where the anticline has a prevalent eastward vergence, shortening in the basement is absorbed by folding in the cover close to the basement fault tip line and the cover thrusts do not reach the surface. We modelled this folding with the trishear model using a low to intermediate *p*/*s* ratio (3.5–6.5). In cross-section 11 there is an important change in the fold development. From this latitude to the south, the Palauco anticline changes vergence from east to west. We interpreted this change to be due to the reactivation of the pre-existing NNW-trending normal fault segments. We modelled the southern part of the anticline with a high value of *p*/*s* (9) in cross-section 11, which slowly diminishes southward.

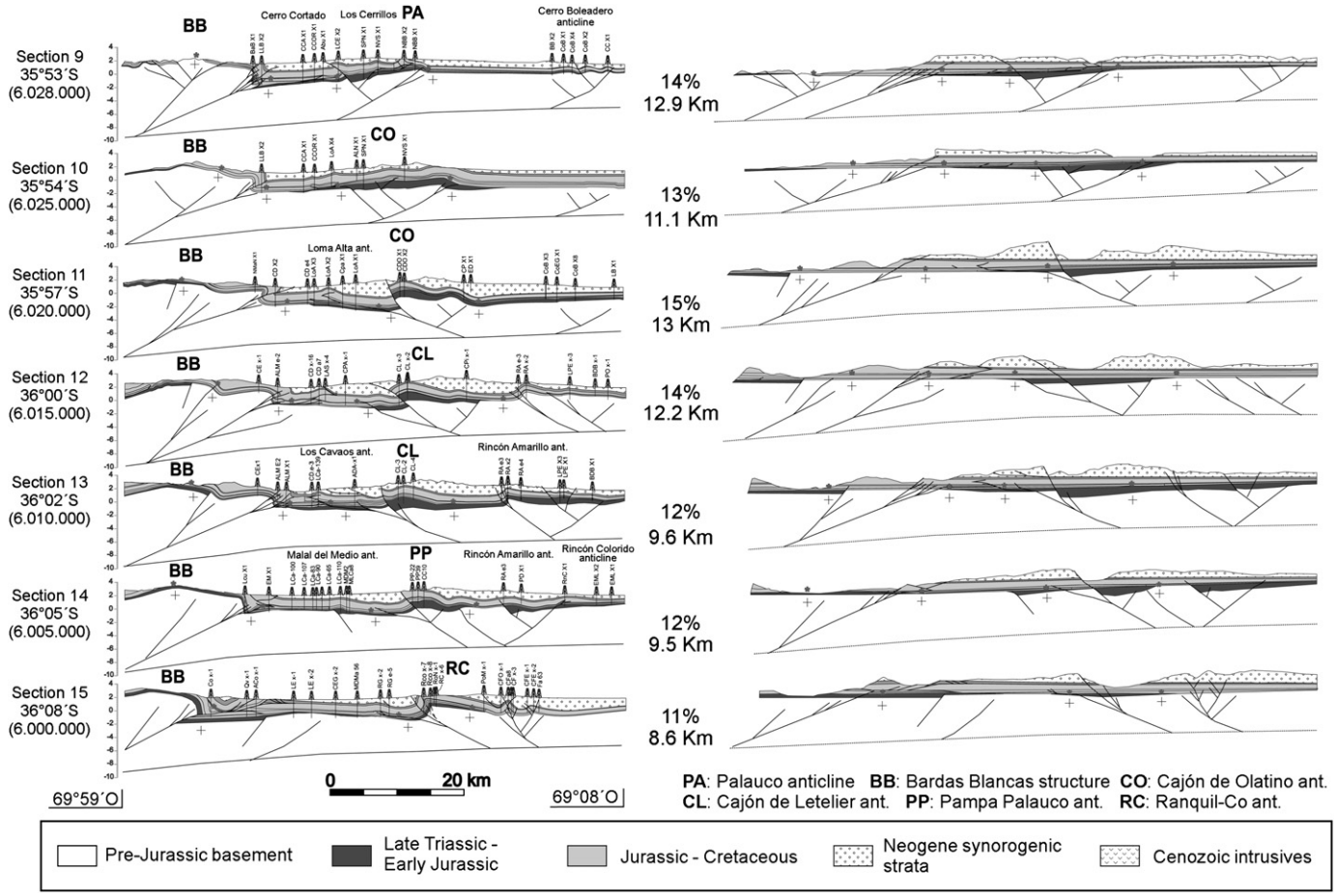


**Fig. 6.** Balanced cross-sections 8–15 in the thrust front of the Malargüe FTB, between 35°52′ and 36°08′S.

### 5.3. *Bardas Blancas fault system*

The Bardas Blancas fault system involves the La Valenciana, Bardas Blancas and Sierra Azul basement structures (Fig. 2). It has been interpreted as a basement-involved complex structure, attributed to the emplacement of the blind Bardas Blancas thrust (Manceda et al., 1992; Dimieri, 1997; Dicarlo and Cristallini, 2007). The fault system contains elements that are consistent with both fault-propagation and fault-bend folding kinematics. It is divided here into three sectors with different kinematics; the northern, central and southern sectors, between cross-section 1 and 8, 9 and 12, and 13 and 15, respectively (Figs. 5 and 6). In the northern sector (Fig. 10), slip from the basement-involved thrusts is transmitted up-section through splays from the principal basement fault. When

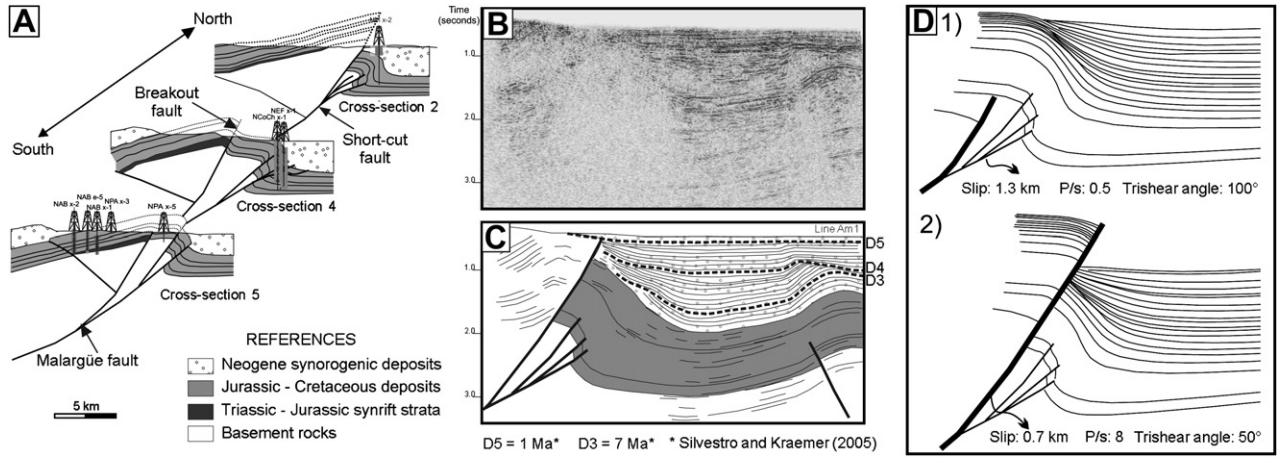


**Fig. 7.** (A) Interpretation of the Malargüe anticline in cross-sections 2, 4 and 5 (Fig. 2). (B) Seismic line of the Malargüe and Chacay anticlines. See location in Fig. 4. (C) Interpretation of the seismic line showing the erosional surfaces postulated by Silvestro and Kraemer (2005). (D) A trishear model for the evolution of the Malargüe anticline in cross-section 2. (1) First episode of compresional deformation with the inversion of the lower sector of the listric normal fault and the development of a short-cut fault folding the cover with a low *p*/*s* ratio. (2) Afterwards, the upper sector of the pre-existing normal fault inverted with a high *p*/*s* ratio.

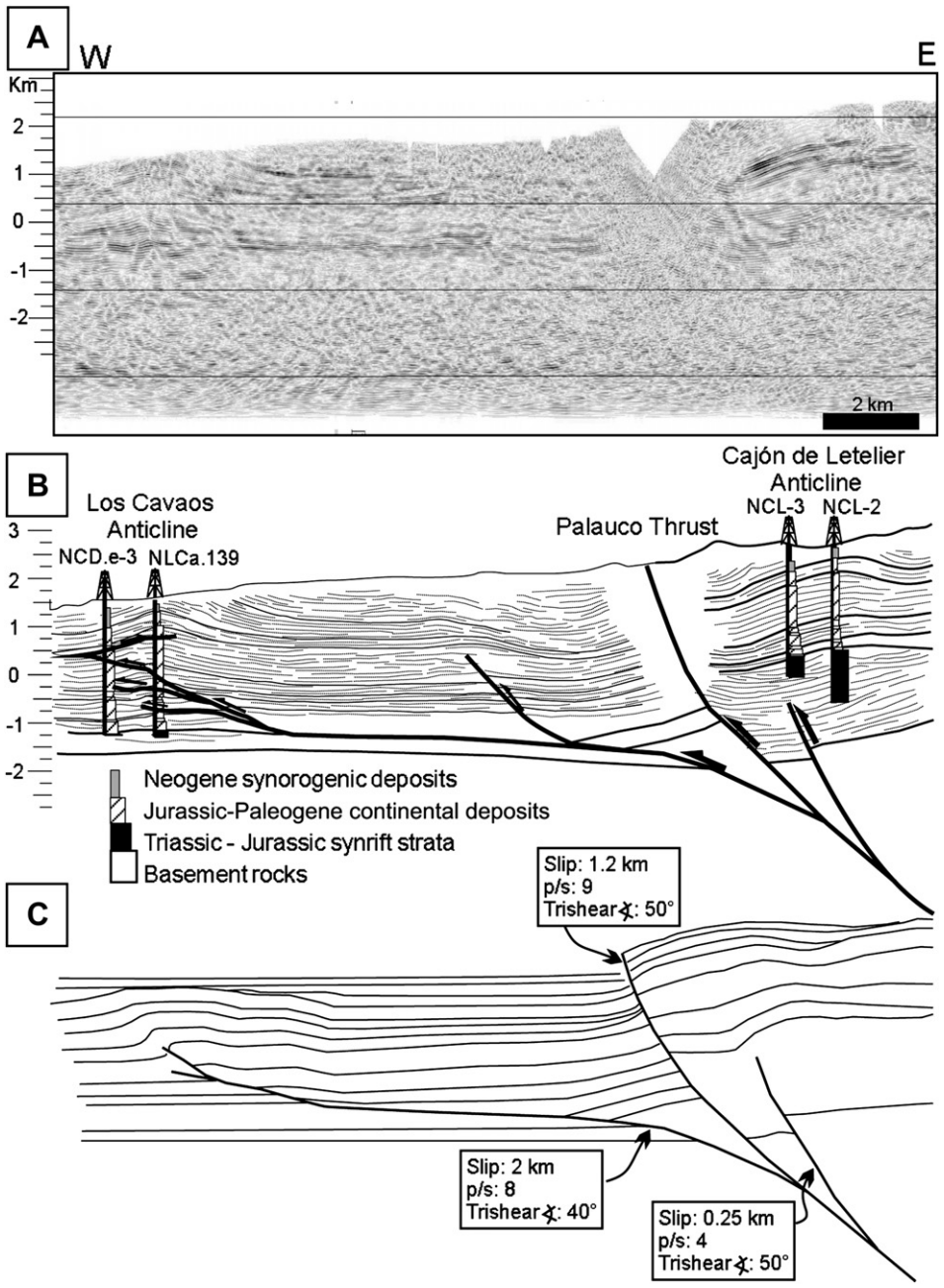


**Fig. 8.** (A) Seismic line B in Fig. 4 – cross-section 13. (B) Interpretation of the seismic line showing the reactivation of the pre-existing Triassic–Jurassic Palauco normal fault. (C) Trishear modelling using high *p*/*s* value for reactivation of the Palauco fault.

these faults cut up-section and propagate from the basement to the cover, they flatten into detachments in the Jurassic shales and the Cretaceous evaporites. The frontal thrusts of the basement-involved structure have a staircase trajectory in which the faults follow bedding-parallel detachments in incompetent horizons and climb upwards through competent units. The basement–cover interface is an undeformed, planar surface which allows us to infer that the fault growth proceeded with an initially rapid propagation and a high *p*/*s* ratio. Subsequent translation of the fold in the hanging wall as slip increased and duplication of strata produced a modified fault-bend fold. After the first stage of shortening, the model of fold-thrust interaction changed from fault-bend to fault-propagation folding. This change is reflected by a decrease in foreland translation. Structures may have initiated as a fault-bend fold with inclined shear deformation at its backlimb and a combination of synthetic inclined shear in the basement rocks and flexural slip in the cover in the forelimb. With progressive shortening, faults would have broken through the forelimb of the basement unit to ride up to the detachment within the Jurassic shales. The geometric modification that occurs in the Bardas Blancas structure could have resulted from strain weakening of the leading portion of the thrusted basement, caused by fracturing and cataclasis during bending. This reduction in hanging wall strength, together with an increase in resistance to foreland translation appears responsible for enhancing thrusting within the basement leading portion.

South of cross-section 8 (Fig. 10), in the central sector, there is a change in fold–fault kinematics from fault-bend to fault-propagation folding. In this sector, the footwall basement–cover

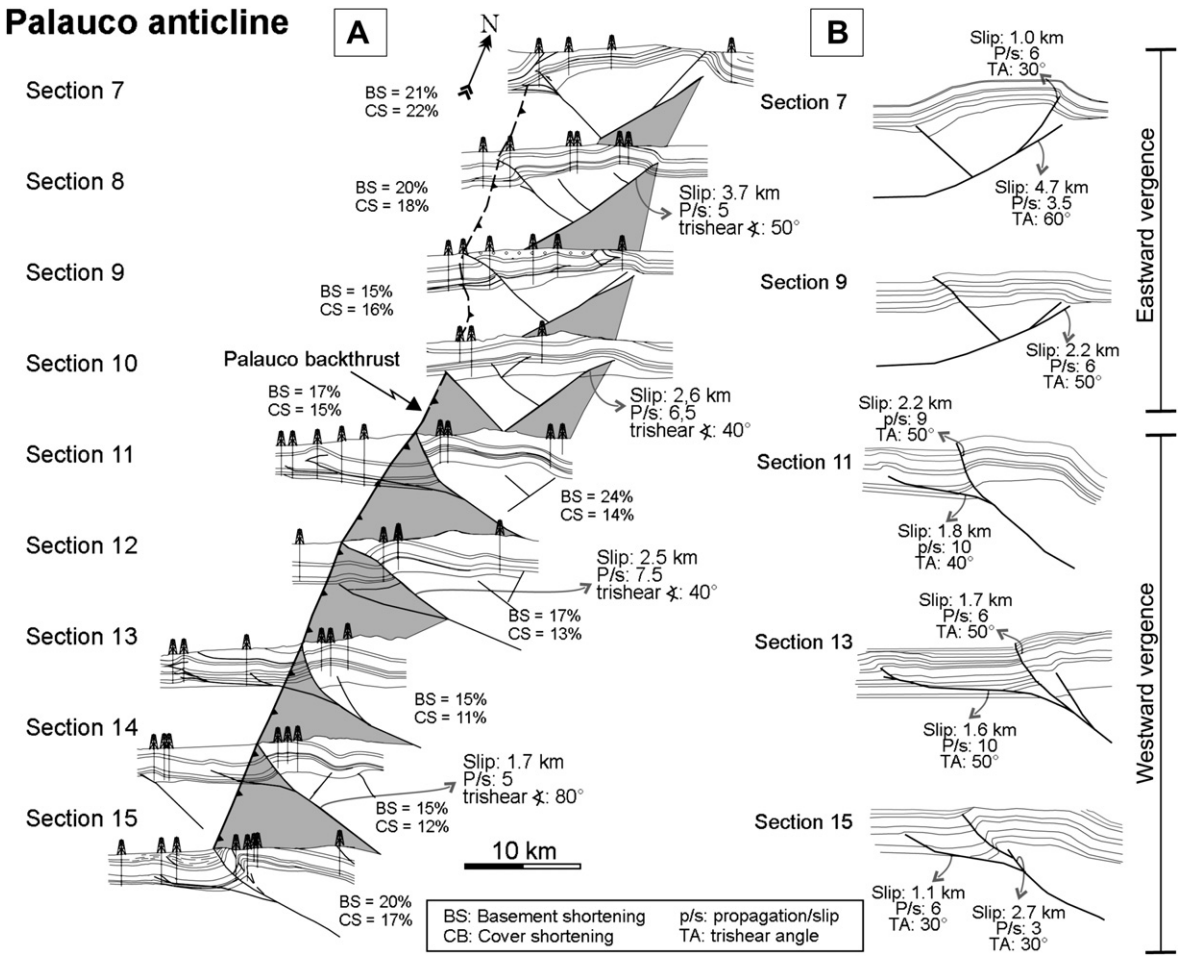


**Fig. 9.** (A) Geometry of the Palauco anticline in cross-sections 7–15 (Fig. 2), and variation of basement–cover shortening and *p*/*s* along strike. The amount of basement shortening is compared with shortening in the cover. (B) Trishear models that fit the basic geometries of cross-sections 7, 9, 11, 13 and 15. Notice that similar percentage of shortening in the basement and cover correlates with low *p*/*s* ratio.

interface is inferred to be folded before being faulted. This is in agreement with fault-propagation folding with low *p*/*s* ratios where layers are folded and then faulted as fault displacement increases.

Between cross-sections 13 and 15, in the southern sector, the mechanism best suitable for modelling the thrust system is fault-bend folding with flexural slip. The *p*/*s* ratio is interpreted to increase gradually towards the south. Shortening in the basement is transferred to the cover, developing a thin-skinned sector in front of the basement structure uplift.

## 6. Three-dimensional distribution of shortening

Homogeneous distributed deformation is a general assumption of models of fold-thrust wedges. Although this assumption may be appropriate for an entire fold and thrust belt, individual fault systems may show heterogeneous distribution of shortening as a result of variation in fault–fold interaction kinematics and the presence of pre-existing structures. Here we will analyse along and across-strike distribution of shortening in the Malargüe FTB and its relation with the fault–fold kinematics.

Balanced cross-sections 1–15 indicate that horizontal shortening varies between 25 and 11%, decreasing toward the south (Figs. 5, 6 and 11A). The lost of 16.6 km of shortening over a distance of about 78 km is equivalent to a differential displacement shear angle of 12°. This loss of displacement is homogenously accommodated by all basement structures across strike, specially the Bardas Blancas basement structure and the Doña Juana – La Brea triangle zone (Fig. 5). The Bardas Blancas fault system experienced the greatest magnitude of shortening, which varies along strike (Fig. 11B, lines 2a and 2b). In this structure, there is an important discrepancy between basement and cover shortening (Fig. 11B, line 2a). In all cross-sections, except cross-sections 9–11, basement shortening, which varies between 72 and 24%, is 10–58% higher than the cover shortening (Fig. 11B, line 2b). This is illustrated in Fig. 11B where the shadow below line 2 is an indication of the amount of this discrepancy. On the contrary, in the Doña Juana-La Brea triangle zone, cover shortening (Fig. 11B, line 3b) is significantly higher than basement shortening (Fig. 11B, line 3a) because it is essentially a thin-skinned structure with little or no basement involvement. This indicates that the mechanism of foreland translation of deformation from basement to cover is very effective in these structures, except in cross-sections 9–11.

On the other hand, the Malargüe anticline shows no significant variation in basement and cover shortening (Fig. 11B, lines 4a and 4b, respectively), indicating that these basement structures are coupled with the sedimentary cover. Shortening in these structures decreases southward with a shallow slope. We interpret this gentle decrease as due to the existence of a pre-existing normal fault, which controlled the Triassic–Jurassic Malargüe half-graben.

Between cross-sections 7 and 10, the Malargüe structure transfers displacement to the Palauco structure, maintaining the

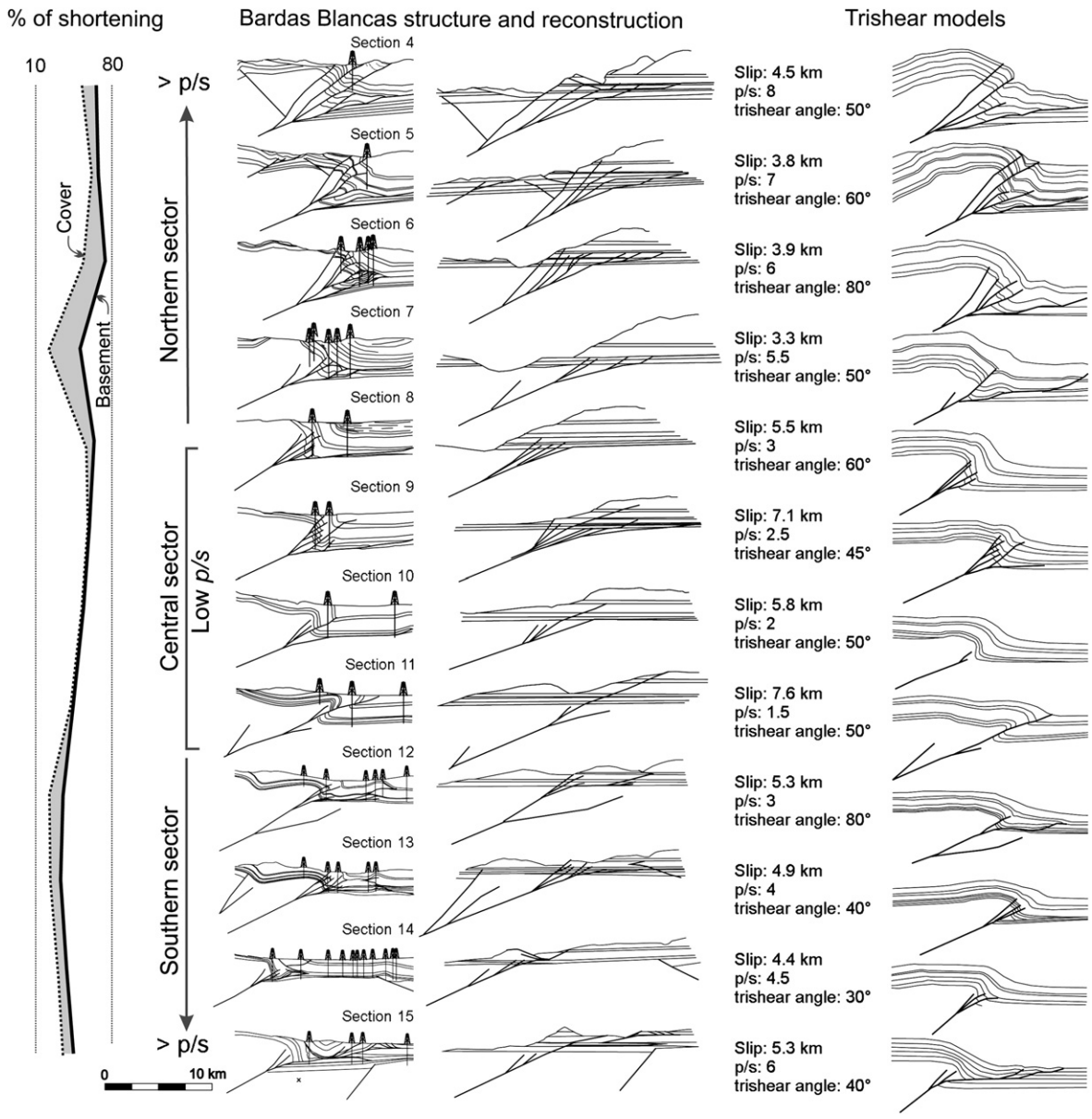


**Fig. 10.** Cross-sections and reconstructions of the Bardas Blancas structure from North to South, showing variations in horizontal shortening in the cover and basement. The trishear models of the broad scale geometries were carried out to analyse variations in trishear parameters, specially the *p*/*s*. Notice correlation between low *p*/*s* and similar percentage of shortening in the basement and in the cover.

total shortening. In this sector, basement and cover amounts of shortening do not differ significantly, indicating that the deformational mechanism is similar to the one in the Malargüe anticline. Southward, in cross-sections 11–15, there is an important discrepancy between basement and cover shortening, indicating that the cover is not welded to the basement. The inferred inverted structures, the Malargüe fault in cross-sections 3–5, and the Palauco fault in cross-sections 10–14, show an amount of horizontal shortening constrained between 12 and 28%. The sector of the Malargüe fault that is not interpreted as inverted (cross-sections 1 and 2) has a shortening close to 40%, suggesting that the presence of high angle normal fault could have limited the total amount of shortening during inversion to up to 28%.

All of these shortening values illustrate that the belt is characterized by inhomogeneous internal shortening parallel to the transport direction and that this heterogeneity cannot be directly correlated with the fault-related fold mechanism or the percentage of shortening.

## 7. Discussion

### 7.1. Coupled and uncoupled basement–cover bonding

Schmidt et al. (1993) postulated two modes for basement-involved structures, one in which basement is deformed primarily by movement on a major fault, whereas the sedimentary cover dissipates the deformation in a triangular zone, and the other with internal deformation of the basement. Following these modes of structures, Mitra and Mount (1998) proposed two end-member models to address the transfer of fault slip to folding in thick-skinned structures, depending on whether the cover units are mechanically homogeneous and welded to the basement or mechanically inhomogeneous and decoupled from the basement. They showed that in the welded cover model the basement deforms primarily by movement on a major fault, where slip is consumed by folding within the sedimentary cover; while in the

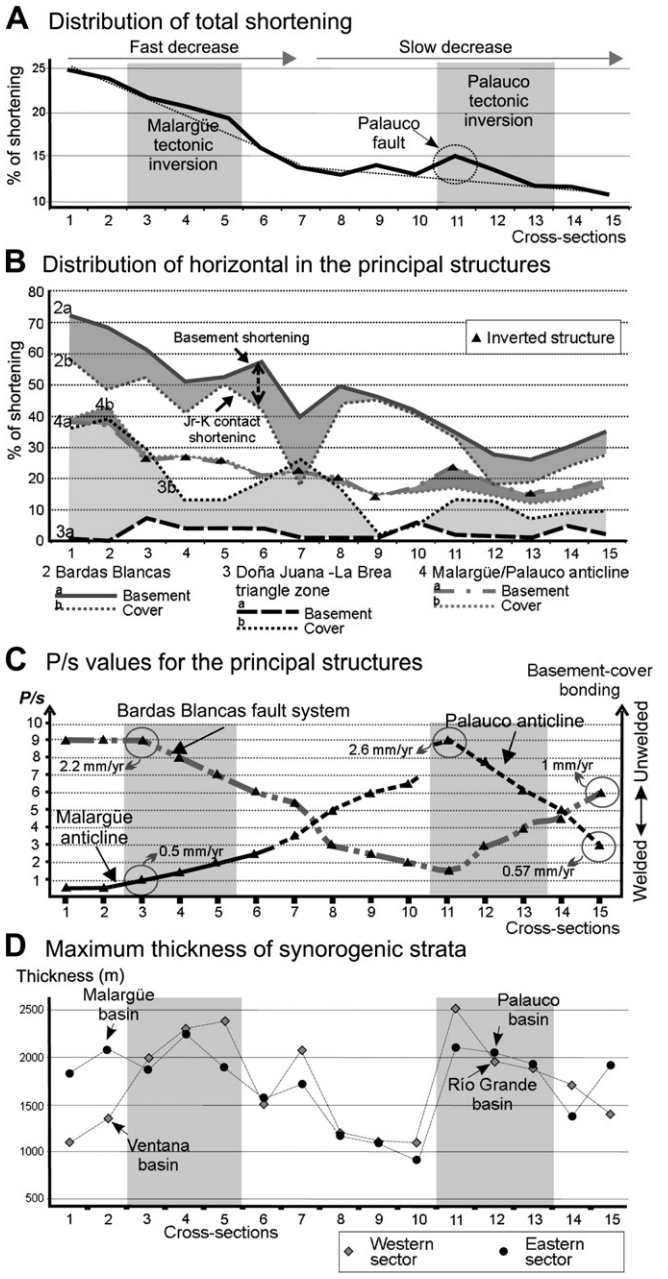


**Fig. 11.** (A) Distribution of horizontal shortening along and across strike in the Malargüe FTB. Notice the influence of reactivation of pre-existing normal structures. (B) Distribution of cover and basement shortening along the principal structures. Continuous lines correspond to percentage of shortening of the basement structures. Dotted lines represent the percentage of shortening of the Jurassic–Cretaceous contact line above the basement structures. The black arrow indicates the discrepancy between basement and cover shortening. This discrepancy is related to the type of fault–fold interaction which promotes or inhibits foreland transference of basement shortening. (C) Diagram illustrating the direct relationship between *p*/*s* and bonding between basement and cover, and the inverse relationship between *p*/*s* values in the western Bardas Blancas structure and the eastern Malargüe–Palauco structures. (D) Variations of synorogenic strata thicknesses along and across strike.

uncoupled model, the basement is detached from the cover by a ductile unit that accommodates the different styles of deformation between the basement and the cover.

Following the classification of Mitra and Mount (1998) for coupled and uncoupled basement–cover bonding, we propose an alternative approach to compare fault geometries and fold shapes for the analysis of fault–fold relations. This approach involves consideration of the distribution of shortening within the basement and cover (Fig. 12). If basement structures are uncoupled from the cover structures, then the discrepancy in shortening between basement and cover can be accommodated by slip in the detachment, passing shortening in the basement onto the foreland cover (Fig. 12A). If basement and cover are coupled, this discrepancy will be less (Fig. 12B). The kind of bonding between basement and cover is also related to the *p*/*s* ratio, because high values of this ratio indicate rapid forward propagation of shortening into the cover (Fig. 12A), while low values favor welding between basement and cover structures (Fig. 12B).

In our field examples, the Bardas Blancas structure corresponds to an unwelded basement–cover bonding, with high *p*/*s* ratio values (6–9) and high discrepancy (up to 58%) between basement and cover shortening, except in its central sector between cross-sections 8 and 11 (Figs 10 and 11B). The kinematic algorithm that is best applied for this kind of bonding is a combination of inclined shear for the basement and flexural slip for the cover. On the contrary, in the Malargüe and northern sector of the Palauco anticlines, the cover is welded to the basement and deformation took place with low *p*/*s* ratios (1–4) and low discrepancy (<10%) between amounts of shortening in the cover and the basement (Fig. 11). The coupled basement–cover bonding is best modelled with the trishear algorithm. Trishear fails if the cover is not perfectly welded to the basement because in this case, there is a discontinuity in velocity at the basement–cover contact (Johnson and Johnson, 2002).

The southern sector of the Palauco anticline has an unwelded basement–cover bonding, coinciding with the change between eastward to westward vergence and the reactivation of the pre-existing normal fault segments. This suggests that the abrupt increase in the *p*/*s* ratio is related to this reactivation.

We find a close inverse correlation of *p*/*s* values between the principal basement structures across strike (Fig. 11C). In cross-sections 1–8, the Bardas Blancas structure has a high value of *p*/*s* while the Malargüe and northern sector of the Palauco anticlines have a low one. Southward, there is a correlation between the abrupt increase in *p*/*s* value for the Palauco structure and a decrease in *p*/*s* values in the Bardas Blancas structure. Likewise, the diminishing of *p*/*s* values for the Palauco anticline towards cross-section 15 is correlated with an increase in the Bardas Blancas structure. We will discuss in the next section factors that could control this inverse correlation between different *p*/*s* values across strike.

### *7.2. Factors controlling the kinematics of basement–cover deformation*

The Malargüe FTB case study sheds insights on the basement–cover interaction mechanisms and the distribution of shortening of individual structures along and across strike. Shortening, *p*/*s* ratio and degree of welding between basement and cover structures greatly vary along and across strike. This variability of geometry and kinematics shows that these geometries are not simple a function of lithological controls but also of other variables. Previous studies have suggested that such variables could be: (1) physical conditions of the deformation (Gangi et al., 1977; Berger and Johnson, 1980; Mitra and Mount, 1998), (2) competency contrast between the basement and cover rocks (Mitra and Mount, 1998), (3) composition and fabric of the basement (Mitra and Mount, 1998), (4) strength and degree of mechanical isotropy in the cover (Chester et al., 1991; Strayer and Hudleston, 1997; Erickson et al., 2001; Johnson and Johnson, 2002; Finch et al., 2003; Strayer et al., 2004; Hardy and Finch, 2006), (5) presence and thickness of growth strata (Strayer et al., 2004), and (6) the geometry of the basement fault (Finch et al., 2003).

Mitra and Mount (1998) proposed that some factors influencing the welded or unwelded basement–cover bonding are the physical

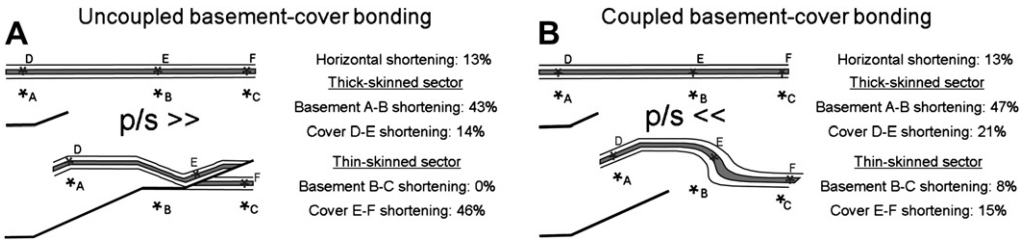


**Fig. 12.** Two end-members of the basement–cover bonding model. (A) Uncoupled model allows forelandward propagation of shortening which generates a discrepancy between basement and cover percentage of shortening. (B) Coupled model inhibits foreland propagation of shortening and results in similar shortening for the basement and cover.

conditions of deformation, such as higher temperatures and pressure which will favour the basement to deform by penetrative deformation or minor faulting, the competency contrast between the basement and overlying units and composition and fabric of the basement (Mitra and Mount, 1998).

The strength of the cover primarily controls the resistance to foreland translation and has a significant effect on the final geometry of fault-related folds (Chester et al., 1991; Strayer and Hudleston, 1997; Hardy and Finch, 2006). Unlimited foreland slip produces an open fault-bend style fold with emergent thrust surface; while if foreland translation is restricted, the forelimb of the resultant fold is vertical to overturned, producing a fault-propagation fold with non-emergent thrust (Strayer et al., 2004). Finch et al. (2003) used discrete element models to investigate the influence of basement fault dip and sedimentary cover strength on the geometry of the fault-propagation folds and the rate of fault propagation. They found that, as the cover strength decreases, the zone of deformation became wider and fold geometries resemble thishear fold profiles with low $p/s$ ratios, typically around 1. In contrast, a stronger cover produces a narrow zone of deformation and more rapid fault propagation, with $p/s$ ratios around 2 or 3. They concluded that the $p/s$ ratio is a gross reflection of the strength of the cover.

Strayer et al. (2004) demonstrated that the presence and thicknesses of growth strata has a significant effect on the final geometry of the associated fault-related folds. Their models show a smooth progression from fault-bend style to fault-propagation style geometry, as growth strata thickness increases. Fault slip goes from being almost completely transferred upward, to being lost upward into an overturned anticline. This indicates that growth strata clearly act as a buttress to the deformation, resisting forelandward translation of the emergent fault-related fold.

Mechanical models suggest that the fault-bend fold mechanism is favourable under the influence of the overburden pressure. In these models, the ramp propagates up and flattens in the basement–cover interface (Gangi et al., 1977; Berger and Johnson, 1980). Another parameter that favours the fault-bend folding mechanism is the existence of an anisotropic mechanical layering of the cover (Chester et al., 1991), because bedding-parallel slip tends to occur in well-layered materials (Erickson et al., 2001). As was pointed out by Erickson (1996), who used elastic–plastic models, the presence of a evaporite décollement is a key factor in producing a fault-bend folding belt.

For our case study, we analyse the diverse factors that have been postulated to influence the kinematic of basement–cover deformation. Physical conditions of deformation, competency contrast between the basement and cover rocks, and composition and pervasive fabric of the basement are almost the same for the Bardas Blancas, Malargüe and Palauco structures. These factors do not change greatly along or across strike, demonstrating that they did not control the fault–fold interaction mechanisms. On the other hand, the nature of the Mesozoic stratigraphic package overlying the basement and its thickness varies across strike from a more than 4 km thick package of competent and incompetent layers in the west to a less than 1 km thick package of competent layers with few incompetent ones to the east (Fig. 3). In the Bardas Blancas structure, the thick shale and evaporite layers underwent penetrative deformation to absorb the fault slip through internal deformation. This is not observed in the eastern sector, where these layers are not present and the Mesozoic package is considerable thinner. This across-strike variation of thickness and anisotropic mechanical layering of the cover strongly influences the geometry of structures in the Malargüe FTB, indicating that it is one of the principal factors controlling changes in fault–fold interactions across strike.

Thicknesses of the synorogenic strata vary along strike, from 2000 m in cross-section 1 to less than 800 in cross-section 10. This decrease is correlated with an increase in $p/s$ values in the Malargüe anticline, suggesting an inverse relation between synorogenic strata thickness and $p/s$ (Fig. 11D). This is not the case for the Palauco anticline, with high values of $p/s$ and more than 2000 m of synorogenic strata, suggesting that another factor controlled the high $p/s$ in this structure.

The timing of deformation of the Bardas Blancas, Malargüe, and Palauco structures was constrained by Silvestro and Kraemer (2005) and Silvestro and Atencio (in press) by the age of synorogenic strata. For the Malargüe anticline they analysed the growth strata onlapping the forelimb of the anticline and proposed that the anticline was active between 7 and 1 Ma (Fig. 7). During the Late Pliocene to Early Pleistocene the fold was broken by the Malargüe thrust, with the movement fossilized under Pleistocene deposits. The main episode of deformation in the Bardas Blancas structure was constrained by these authors between 15.8 and 6.7 Ma in cross-section 3, and 17 and 11 Ma in cross-section 15. They constrained deformation in the Palauco anticline in cross-section 11 between 10.8 and 8.14 Ma, and in the Ranquil-Co anticline (cross-section 15–Fig. 6) between 17 and 10. With these values we calculated the strain rate for the Malargüe and Bardas Blancas structures in cross-section 3 and obtained strain rates of 0.5 and 2.2 mm/yr respectively. The Palauco anticline shortened 7 km in cross-section 11, indicating a high strain rate of 2.6 mm/yr. On the other hand, the southern culmination of this structure, in the Ranquil-Co area, 4 km of shortening was achieved with a strain rate of 0.5 mm/yr. In the same cross-section, the Bardas Blancas structure shortened 7 km between 17 and 11 Ma (1 mm/yr). Low strain rates in Malargüe and Ranquil-Co structures and high strain rates in Bardas Blancas (cross-section 3) and Palauco (cross-section 11) can be related to low and high $p/s$ values, respectively, and this suggests a close relation between strain rates and fault–fold mechanisms.

Thickness and mechanical anisotropy of the cover, thickness of the synorogenic strata, and slip rates could account for the across-strike variations in kinematics between the Bardas Blancas structure and the Malargüe and Palauco anticlines, but could not account

for the along strike variations in these structures. A fourth factor that could have played a role in the variation of deformational style, both along and across strike, is the presence and geometry of pre-existing normal faults, such as the Palauco and Malargüe faults. The Palauco fault is interpreted to have been reactivated during Cenozoic contraction and is related to the abrupt increase in the *p*/*s* ratio of the Palauco structure. The Malargüe fault, on the other hand, is interpreted to have a listric geometry which could have prevented the inversion of its upper part, producing an associated low *p*/*s* short-cut fault.

## 8. Conclusions

We have investigated through natural examples from the Malargüe fold and thrust belt, the manner in which the basement structures interact with the cover in a thick-skinned fold and thrust belt. The Malargüe FTB has experienced different deformation mechanisms resulting in a hybrid fold–fault style along and across the strike. Fault-bend folding is associated with high *p*/*s* ratio and antithetic oblique shear deformation in the backlimb of basement folds and flexural slip within the sedimentary cover; while trishear fault-propagation folding is related to low *p*/*s* values. Although the first mechanism of deformation predominates in the internal sector of the belt, while trishear deformation describes the external structures, some structures in the internal sector of the belt show trishear-like mechanisms and this is correlated with fault-bend folding in their external sectors.

Our work suggests that there is a broad spectrum of basement–cover interaction mechanisms with two end-members: coupled and uncoupled interactions. These interactions are related to the *p*/*s* ratio, and the discrepancy between basement and cover shortening, but they are not directly related to amount of shortening. Factors controlling these types of interactions are inferred to be the (i) mechanical anisotropy and thickness of the cover, (ii) slip rate, (iii) synorogenic strata thickness, and (iv) presence and geometry of pre-existing basement faults. The mechanical anisotropy in the cover promotes flexural slip deformation associated with a weak basement–cover interaction, while a more isotropic cover would promote trishear deformation in the cover and strong basement–cover interaction. A relative high slip rate could favour a fault-bend fold mechanism with high *p*/*s* ratio and weak basement–cover interaction, while a relative low slip rate could favour a fault-propagation fold mechanism, with low *p*/*s* ratio and a strong interaction. This last mechanism would be favourable with thick synorogenic strata. Pre-existing structures are generally associated with high *p*/*s* values, because the propagation of the fault occurred in a previous event. However, pre-existing highly dipping listric normal faults could have prevented inversion during the Cenozoic compression and instead promoted the development of a short-cut fault in the shallow levels of the basement with an associated low *p*/*s*.

## Acknowledgements

This research was supported by grants from the Agencia Nacional de Promoción Científica y Tecnológica (PICT 07-10942) and CONICET (PIP 5843). We wish to thank Repsol-YPF for authorization to publish data. Two anonymous reviewers are sincerely thanked for their critical and helpful comments and suggestions.

## References

Allmendinger, R.W., 1998. Inverse and forward numerical modeling of trishear fault-propagation folds. Tectonics 17, 640–656.

Allmendinger, R.W., Shaw, J., 2000. Estimation of fault propagation distance from fold shape: implications for earthquake hazard assessment. Geology 28, 1099–1102.

Allmendinger, R.W., Zapata, T.R., Manceda, R., Dzelalija, F., 2004. Trishear kinematic modeling of structures with examples from the Neuquén Basin, Argentina. In: McClay, K.R. (Ed.), Thrust Tectonics and Hydrocarbon Systems. American Association of Petroleum Geologists, Memoir, vol. 82, pp. 356–371.

Berger, P., Johnson, A.M., 1980. First-order analysis of deformation of a thrust sheet moving over a ramp. Tectonophysics 70, 9–24.

Buddin, T.S., Kane, S.J., Williams, G.D., Egan, S.S., 1997. A sensitivity analysis of 3-dimensional restoration techniques using vertical and inclined shear constructions. Tectonophysics 269, 33–50.

Bulnes, M., McClay, K.R., 1998. Structural analysis and kinematic evolution of the inverted central South Celtic Sea Basin. Marine and Petroleum Geology 15, 667–687.

Cardozo, N., Bawa-Bhall, K., Zehnder, A., Allmendinger, R.W., 2003. Mechanical models of fault propagation folds and comparison to the trishear kinematic model. Journal of Structural Geology 25, 1–18.

Cardozo, N., Allmendinger, R.W., Morgan, J.K., 2005. Influence of mechanical stratigraphy and initial stress state on the formation of two fault propagation folds. Journal of Structural Geology 27, 1954–1972.

Chester, J., Chester, F., 1990. Fault propagation folds above thrusts with constant dip. Journal of Structural Geology 12, 903–910.

Chester, J.S., Logan, J.M., Spang, J.H., 1991. Influence of layering and boundary conditions on fault-bend and fault-propagation folding. Geological Society of America, Bulletin 103, 1059–1072.

Dessanti, R.N., 1973. Descripción geológica de la Hoja 29b Bardas Blancas (Provincia de Mendoza). In: Servicio Nacional Minero Geológico, Boletín 139.

Dicarlo, D.J., Cristallini, E., 2007. Estructura de la margen norte del río Grande, Bardas Blancas, Provincia de Mendoza. Revista de la Asociación Geológica Argentina 62, 187–199.

Dimieri, L.V., 1997. Tectonic wedge geometry at Bardas Blancas, southern Andes (36°S), Argentina. Journal of Structural Geology 19, 1419–1422.

Dula, W.F., 1991. Geometric models of listric normal faults and rollover folds. American Association of Petroleum Geologists, Bulletin 75, 1609–1625.

Egan, S.S., Kane, S., Buddin, T.S., Williams, G.D., Hodgetts, D., 1999. Computer modeling and visualization of the structural deformation caused by movement along geological faults. Computers and Geosciences 25, 283–297.

Erickson, G., 1996. Influence of mechanical stratigraphy on folding vs faulting. Journal of Structural Geology 18, 443–450.

Erickson, G., Strayer, L.M., Suppe, J., 2001. Initiation and reactivation of faults during movement over a thrust-fault ramp: numerical mechanical models. Journal of Structural Geology 23, 11–23.

Erslev, E.A., 1991. Trishear fault-propagation folding. Geology 19, 617–620.

Erslev, E.A., Rogers, J.L., 1993. Basement-cover geometry of Laramide fault-propagation folds. In: Schimdt, C.J., Chase, R.B., Erslev, E.A. (Eds.), Laramide basement deformation in the Rocky Mountain foreland of the western United States. Geological Society of America, Special Publication, vol. 280, pp. 125–146.

Farías, M., Charrier, R., Comte, D., Martinod, J., Hérail, G., 2005. Late Miocene high and rapid surface uplift and its erosional response in the Andes of central Chile (33°–35°S). Tectonics 27, TC1005. doi:10.1029/2006TC002046.

Finch, E., Hardy, S., Gawthorpe, R.L., 2003. Discrete element modeling of contractional fault-propagation folding above rigid basement fault blocks. Journal of Structural Geology 25, 515–528.

Ford, M., Williams, E.A., Artoni, A., Vergés, J., Hardy, S., 1997. Progressive evolution of a fault-related fold pair from growth strata geometries, San Llorenc de Morunys, SE Pyrenees. Journal of Structural Geology 19, 413–441.

Gangi, A.F., Min, K.D., Logan, J.M., 1977. Experimental folding of rocks under confining pressure: part IV – theoretical analysis of faulted drape-folds. Tectonophysics 42, 227–260.

Giambiagi, L., Bechis, F., García, V., Clark, A., 2008. Temporal and spatial relationship between thick- and thin-skinned deformation in the Malargüe fold and thrust belt, southern Central Andes. Tectonophysics 459, 123–139.

Giambiagi, L., Tunik, M., Barredo, S., Bechis, F. y Ghiglione, M. Cinemática de apertura del sector mendocino de la cuenca Neuquina. Revista de la Asociación Geológica Argentina, in press.

Groeber, P., 1937. Mapa Geológico de la Hoja 30c (Puntilla de Huincán) del mapa Geológico General de la República Argentina. Dirección Nacional de Minería y Geología.

Gulisano, C., Gutierrez Pleimling, A., 1994. Field trip guidebook, Neuquina Basin, Mendoza Province. In: Fourth International Congress on Jurassic Stratigraphy and Geology, 103 pp.

Hardy, S., 1997. A velocity description of constant-thickness fault-propagation folding. Journal of Structural Geology 19, 893–896.

Hardy, S., Allmendinger, R. Trishear: a review of kinematics, mechanics and applications. American Association of Petroleum Geologists, Special Publication, in press.

Hardy, S., Finch, E., 2006. Discrete element modeling of the influence of cover strength on basement-involved fault-propagation folding. Tectonophysics 415, 225–238.

Hardy, S., Finch, E., 2007. Mechanical stratigraphy and the transition from trishear to kink-band fault-propagation fold forms above blind basement thrust faults: a discrete-element study. Marine and Petroleum Geology 24, 75–90.

Hardy, S., Ford, M., 1997. Numerical modeling of trishear fault-propagation folding. Tectonics 16, 841–854.

Hardy, S., Poblet, J., 1995. The velocity description of deformation. Paper 2: sediment geometries associated with fault-bend and fault-propagation folds. Marine and Petroleum Geology 12, 165–176.

Hedlund, C.A., 1997. Fault-propagation, ductile strain, and displacement–distance relationships. Journal of structural Geology 19, 249–256.

Jamison, W.R., 1987. Geometric analysis of fold development in overthrust terranes. Journal of Structural Geology 9, 207–219.
Johnson, K.M., Johnson, A.M., 2002. Mechanical analysis of the geometry of forced-folds. Journal of Structural Geology 24, 401–410.
Kane, S.J., Williams, G.D., Buddin, T.S., Egan, S.S., Hodgetts, D., 1997. Flexural-slip Based Restoration in 3D, A New Approach. American Association of Petroleum Geologists. Annual Convention Official Program: A58.
Kozlowski, E., Cruz, C., Condat, P., Manceda, R., 1989. Informe geológico zona Malargüe Occidental. YPF. Unpublished Report, Buenos Aires, Argentina.
Kozlowski, E., Manceda, R., Ramos, V.A., 1993. Estructura. In: Ramos, V. (Ed.), Geología y recursos naturales de Mendoza. Relatorio. 12°Congreso Geológico Argentino y 2°Congreso Exploración Hidrocarburos, pp. 235–256.
Legarreta, L., Kokogian, D., Boggetti, D., 1985. Informe Sierra de Palauco. Estratigrafía. Provincia de Mendoza. YPF. Unpublished Report, Buenos Aires, Argentina.
Manceda, R., Figueroa, D., 1995. Inversion of the Mesozoic Neuquén rift in the Malargüe fold-thrust belt, Mendoza, Argentina. In: Tankard, A.J., Suárez, R., Welsink, H.J. (Eds.), Petroleum Basins of South America. American Association of Petroleum Geologists, Memoir, vol. 62, pp. 369–382.
Manceda, R., Bolatti, N.D., Manoni, R., 1992. Modelo estructural para la zona de Bardas Blancas. Boletín de Informaciones Petroleras 9 (31), 32–103.
Mitra, S., 1990. Fault-propagation folds: geometry, kinematic evolution, and hydrocarbon traps. Bulletin of the American Association of Petroleum Geologists 74, 521–531.
Mitra, S., Mount, van S., 1998. Foreland basement-involved structures. American Association of Petroleum Geologists 82, 70–109.
Muraoka, H., Kamata, H., 1983. Displacement distribution along minor fault traces. Journal of Structural Geology 5, 395–483.
Nocioni, A.D., 1996. Estudio structural de la faja plegada y corrida de la Cuenca Neuquina-Surmendocina. 13°Congreso Geológico Argentino y 3°Congreso de Exploración de Hidrocarburos, Buenos Aires. Actas 2, 353–372.
Sanderson, D.J., 1982. Models of strain variation in nappes and thrust sheets; a review. Tectonophysics 88, 201–233.
Schmidt, C.J., Genovese, P.W., Chase, R.B., 1993. Role of basement fabric and cover-rock lithology on the geometry and kinematics of twelve folds in the Rocky Mountain foreland. In: Schimdt, C.J., Chase, R.B., Erslev, E.A. (Eds.), Laramide Basement Deformation in the Rocky Mountain Foreland of the Western United States. Geological Society of America, Special Publication, vol. 280, pp. 1–44.
Silvestro, J., Kraemer, P., 2005. Evolución tecto-sedimentaria de la Cordillera Principal en el sector surmendocino a los 35°30′S. Faja Plegada de Malargüe. República Argentina. 6°Congreso de Exploración y desarrollo de hidrocarburos. Proceedings in CD.
Silvestro, J., Atencio, M. La Cuenca Cenozoica del Río Grande y Palauco: edad, evolución y control estructural. Faja Plegada de Malartüe (36°S). Revista Asociación Geológica Argentina, in press.
Silvestro, J., Kraemer, P., Achilli, F., Brinkworth, W., 2005. Evolución de las cuencas sinorogénicas de la Cordillera Principal entre 35° y 36°S, Malargüe. Revista Asociación Geológica Argentina 60, 627–643.
Strayer, L.M., Hudleston, P.J., 1997. Numerical modeling of fold initiation at thrust ramps. Journal of Structural Geology 19, 551–566.
Strayer, L.M., Erickson, S.G., Suppe, J., 2004. Influence of growth strata on the evolution of fault-related folds: distinct-element models. In: McClay, K.R. (Ed.), Thrust Tectonics and Hydrocarbon Systems. American Association of Petroleum Geologists, Memoir, vol. 82, pp. 413–437.
Suppe, J., 1983. Geometry and kinematics of fault-bend folding. American Journal of Science 283, 684–721.
Suppe, J., Medwedeff, D.A., 1984. Fault-propagation folding. Geological Society of America, Abstracts with Programs 16, 670.
Suppe, J., Medwedeff, D.A., 1990. Geometry and kinematics of fault-propagation folding. Eclogae Geologicae Helvetiae 83, 409–454.
White, N.J., Jackson, J.A., McKenzie, D.P., 1986. The relationship between the geometry of normal faults and that of the sedimentarylayers in their hanging walls. Journal of Structural Geology 8, 897–909.
Wichkam, J., 1995. fault displacement-gradient folds and the structure at Lost Hills, California (U.S.A). Journal of Structural Geology 17, 1293–1302.
Williams, G.D., Chapman, T.J., 1983. Strains development in the hanging wall of thrusts due to their slip/propagation rate: a dislocation model. Journal of Structural Geology 5, 563–571.
Withjack, M.O., Peterson, E.T., 1993. Prediction of normal-fault geometries: a sensitivity analysis. American Association of Petroleum Geologists, Bulletin 77, 1860–1873.
Yagupsky, D., Cristallini, E., Zamora Valcarce, G., Varadé, R., 2007. Sistema compresivo sobreimpuesto a un rift oblicuo: aplicaciones en la faja plegada y corrida de Malargüe, sur de Mendoza. Revista Asociación Geológica Argentina 62, 124–138.
Yagupsky, D., Cristallini, E., Fantín, J., Zamora Valcarce, G., Bottesi, G., Varadé, R., 2008. Oblique half-graben inversion of the Mesozoic Neuquén rift in the Malargüe fold and thrust belt, Mendoza, Argentina: new insights from analogue models. Journal of Structural Geology 30, 839–853.
Zapata, T., Folguera, A., 2005. Tectonic evolution of the Andean fold and thrust belt of the southern Neuquén basin, Argentina. In: Veiga, G.D., Spalletti, L.A. (Eds.), The Neuquén Basin, Argentina: A Case Study in Sequence Stratigraphy and Basin Dynamics. Geological Society of London, Special Publications, vol. 252, pp. 37–56.
Zehnder, A.T., Allmendinger, R.W., 2000. Velocity field for the trishear model. Journal of Structural Geology 22, 1009–1014.